npj | climate and atmospheric science

Article

Published in partnership with CECCR at King Abdulaziz University

https://doi.org/10.1038/s41612-024-00689-z

The dominant factor in extreme dust events over the Gobi Desert is shifting from extreme winds to extreme droughts

Qingzhe Zhu [1,2] & Yuzhi Liu [3,4] ✉

Gobi Desert (GD) is one of the major global dust sources, where dust events are frequent. Based on satellite observations, we compiled extreme dust events (EDEs) over the GD during spring since 2000. Among all 43 extreme events, EDEs on 4–10 April 2001 (EDE 2001) and 14–19 March 2021 (EDE 2021) are the most pronounced, due to the longest duration and the most intense strength, while the generation mechanisms underlying these two EDEs are different. EDE 2001 is associated with extreme westerlies, which are caused by an abnormal low-pressure due to the extreme Eurasian teleconnection (EU). However, EDE 2021 is attributable to extreme droughts, which are caused by an abnormal high-pressure due to the extreme Arctic Oscillation (AO) and West Pacific teleconnection (WP). Moreover, the trends in EU, AO, and WP combined with the analysis of all EDEs indicate a shift in the dominant factor of EDEs over the GD from extreme winds to extreme droughts. Therefore, regional droughts should be given more importance in future EDE forecasts.

Extreme weather events are becoming more frequent under the influence of climate change. In recent years, extreme weather events such as extreme high temperatures, extreme cold snaps, and extreme rainfall have become more severe in terms of intensity, duration, and impact scale, threatening human health, economic stability, and ecological security at regional and global scales[1–3]. Therefore, the occurrence and variations of extreme weather events and their influencing factors have become one of the major scientific challenges of the World Climate Research Programme, and a major scientific issue of general concern to the scientific community, governments, and the public[4,5].

In desert regions, extreme dust events (EDEs) have also occurred repeatedly in recent years, such as a record-breaking trans-Atlantic African dust event that occurred on 14–28 June 2020, greatly degrading air quality over North America[6], and EDEs have also occurred in the Middle East and India[7,8]. Moreover, the Gobi Desert (GD), located on the border of China and Mongolia, is one of the major global dust sources, and EDEs over the GD have also become more severe in recent years. The EDE over the GD in March 2021 caused North China to experience the strongest sandstorm process in nearly a decade[9,10], and in March 2023, the GD experienced another EDE[11,12]. These EDEs over the GD have significantly worsened air quality, reduced visibility, and threatened human health, with far-reaching impacts on the environment, weather, and climate in China, Mongolia, and even East Asia[13–15].

Recent studies reported that EDEs over the GD in 2021 and 2023 were associated with windy weather and arid surface conditions. The Mongolian cyclone and cold high pressure are key factors in windy weather, and the little rainfall and poor vegetation cover over the GD provided dust source conditions[11,16,17]. Related mechanisms are mainly the latitudinal distribution of large-scale circulations due to Arctic sea ice anomalies, combined with strong East Asian winter monsoons caused by sea surface temperature (SST) anomalies leading to moisture dispersion and low rainfall[10]. In addition, several severe sandstorms over the GD at the beginning of this century were at the peak of the La Niña event which strengthened the East Asian winter monsoon, weakened precipitation, and caused frequent strong winds as well as arid surface over the north East Asia, providing powerful conditions for strong dust storms[18].

As mentioned above, current researches on EDEs over the GD mainly focus on the analysis of individual cases, their conclusions are consistent, indicating that strong winds and droughty surface are important factors in the generation of EDEs. Regarding the former, dust particles are mobilized when the near-surface wind speed exceeds the threshold. Surface properties mainly include soil moisture, soil water, and vegetation cover. The droughty

[1]Frontier Science Center for Deep Ocean Multispheres and Earth System (FDOMES) and Physical Oceanography Laboratory, Ocean University of China, 266100 Qingdao, China. [2]Department of Marine Meteorology, College of Oceanic and Atmospheric Sciences, Ocean University of China, 266100 Qingdao, China. [3]Key Laboratory for Semi-Arid Climate Change of the Ministry of Education, Lanzhou University, 730000 Lanzhou, China. [4]Collaborative Innovation Center for Western Ecological Safety, Lanzhou University, 730000 Lanzhou, China. ✉e-mail: liuyzh@lzu.edu.cn

surface causes looser soils and surface particles are more easily entrained into the atmosphere, providing rich material conditions for EDEs. In addition, extreme droughts are the physical basis for dust emissions, and dust is produced mainly in dry and bare surface. Extreme winds affect both dust emissions and dust transport, leading to the effects of EDEs more widespread and longer lasting. In the context of climate change, wind speeds in mid-latitudes are weakening, while droughts are intensifying[19–21]. However, due to the lack of statistical and comparative analyses over a long time series, it is unclear whether the relative importance of winds and droughts on EDEs has changed under climate change. Accordingly, based on satellite observations, we counted the EDEs that occurred over the GD since 2000 and provided the duration and intensity of each EDE. Moreover, by analyzing the two EDEs with the longest duration and highest intensity, we investigated the generation mechanism of EDEs over the GD. Furthermore, combining the analysis of all EDEs, the shift in the dominant factors of EDEs was proposed. We anticipate that our findings will offer insights into the long-term characteristics of EDEs over the GD and enhance the understanding of the variation in EDE driving factors.

Results

EDEs over the GD and corresponding abnormal meteorological patterns

Figure 1a shows the statistical results of EDE over the GD during the spring of 2000–2023, and it is obvious that two long-term and high-intensity EDEs occurred during 4–10 April 2001 (EDE 2001) and 14–19 March 2021 (EDE 2021). The distribution of averaged dust aerosol optical depth (DOD) during these two EDEs is shown in Fig. 1b and c, respectively, which indicates that the dust in these two EDEs mainly occurred over the southern GD. Moreover, the averaged DOD during these two EDEs reached the 99th percentile of daily DOD during the spring from 2000 to 2023 over most areas of the GD (Fig. 1d, e), implying EDE 2001 and EDE 2021 are the strongest EDEs since 2000.

To understand the causes of these two EDEs, the relevant meteorological and land conditions were analyzed. Due to the duration of these two EDEs being approximately 7 days, the conditions during the EDE as well as 2 weeks (week-2) and 1 week (week-1) before extreme events are selected. Two weeks (21–27 March 2001) before EDE 2001, the geopotential height at 500 hPa (G500) was anomalously weak with abnormal northwest winds over the GD (Supplementary Fig. 1a1). However, it reversed one week later, the GD was dominated by anomalously high pressures one week before the event (28 March-3 April 2001; Supplementary Fig. 1a2). During EDE 2001, the GD was once again controlled by low pressure, accompanied by strong westerly wind anomalies (Supplementary Fig. 1a3). The circulation distribution of the EDE 2001 and that of the same period averaged from 2000 to 2023 indicate that the GD was dominated by the westerly winds during 4–10 April (Supplementary Fig. 2a3, b3). In contrast, the GD was dominated by anomalous high pressure during EDE 2021 and two weeks before EDE 2021. The anomalous high pressure was strongest one week before the extreme event. In addition, northeasterly wind anomalies occurred over the GD during EDE 2021 (Supplementary Fig. 1b1–b3 and Supplementary Fig. 3).

Anomalous low pressure resulted in anomalously high 10-m wind speeds (UV10) over the GD during EDE 2001 (Fig. 2a; Supplementary Fig. 4a1, b1) which can provide strong dynamic conditions for dust emission and spread, while UV10 during EDE 2021 was close to the long-term average value due to relatively abnormal high pressure (Fig. 2b; Supplementary Fig. 4a2, b2). The averaged UV10 over the GD during EDE 2001 was the strongest in the same period from 2000 to 2023, which was $+2.26\ m\ s^{-1}$ with respect to the mean of 2000–2023 (Fig. 3a), but that during the EDE 2021 was on the low side of the 2000–2023 period (Fig. 3b). In addition, the average UV10 in EDE 2001 was the strongest during 1 March-10 April 2001 (Supplementary Fig. 5a). Therefore, extremely strong wind is a key factor for EDE 2001, but not for EDE 2021.

Furthermore, corresponding to changes in pressure, the skin temperature (ST) was relatively low in two weeks before EDE 2001, followed by abnormally high ST in 2001 week-1 and cooling during EDE 2001 (Fig. 2c1–c3). In 2021 week-1, abnormally high ST also occurred over the GD (Fig. 2d2), which was substantially stronger than that in 2001 week-1. In addition, relatively high ST also appeared in 2021 week-2 (Fig. 2d1) and ST returned to normal during EDE 2021 (Fig. 2d3). The time series of averaged ST over the GD during the periods contemporaneous with 2001 week-1 and 2021 week-1 from 2000 to 2023 imply that the ST during 2021 week-1 was the highest in the same period from 2000 to 2023, which was +5.15 °C with respect to the mean of 2000–2023 (Fig. 3d), while the ST during 2001 week-1 was the fourth highest during 2000–2023 (Fig. 3c). Moreover, the average ST in 2021 week-1 was the highest during 1 March-10 April 2021 (Supplementary Fig. 5b). Therefore, extreme high ST during pre-EDE, as opposed to wind speed, is critical for EDE 2021.

The relatively high ST in 2001 week-1 resulted in relatively high soil temperatures as well as comparatively low soil water and precipitation over the GD, which in turn caused relatively strong droughts and further contributed to the low snow cover and comparatively sparse vegetation (Fig. 3e). Climate change has facilitated a positive feedback loop between soil moisture deficiency and surface warming over the GD related to drought. Soil moisture deficits impede the cooling effect of evapotranspiration, thus allowing heat to be transferred directly to the air and exacerbating surface warming, which in turn accelerates soil drying. Furthermore, the extremely high ST in 2021 week-1 results in extreme drought over the GD, which is reflected in the highest soil temperatures, the lowest soil water and snow cover as well as the second lowest arid index (AI) and normalized difference vegetation index (NDVI) (Fig. 3f). These features create a dry and loose surface providing substantial material conditions for dust production. Although the wind during EDE 2021 is not strong, these extreme surface features are enough to promote dust generation. Consequently, the EDE in 2021 can be attributed to extreme droughts due to extremely high ST, while the EDE 2001 was mainly caused by extreme winds.

Potential mechanisms affecting strongest EDEs

According to the main factors related to EDE 2001 and EDE 2021, we calculated the regression between time series of UV10 anomalies during the same period as EDE 2001 from 2000–2023 (shown in Fig. 3a) and G500, as well as the regression between time series of ST anomalies during the same period as 2021 week-1 from 2000–2023 (shown in Fig. 3d) and G500. As shown in Fig. 4a1, the UV10 over the GD is closely related to the abnormal low pressure over the desert. In addition, the related wave activity flux indicates that this low pressure is affected by the abnormally high pressure over the Eastern European Plain. Fig. 4a2 indicates that the ST over the GD is attributed to the abnormal high pressure over the desert which is affected by the abnormal low pressure over the Arctic. To further analyze the causes of the above circulations, SST anomalies associated with extreme events are analyzed. As depicted in Supplementary Fig. 6, partially anomalously high SSTs occurred over the North Atlantic during EDE 2001, and anomalously high SSTs occurred over the North Pacific during 2021 week-1. Moreover, the regression between the time series of UV10 anomalies and SST, as well as the regression between the time series of ST anomalies and SST also imply that the UV10 associated with EDE 2001 is influenced by warmer North Atlantic SSTs, while the ST associated with EDE 2021 is affected by warmer North Pacific SSTs (Fig. 4b1 and b2).

Furthermore, the years of the top 5 (top 20%) highest averaged SSTs contemporaneous with EDE 2001 over the North Atlantic and those contemporaneous with 2021 week-1 over the North Pacific from 2000 to 2023 were selected (Supplementary Table 1). Compared with the mean geopotential height at 200 hPa (G200), the Rossby wave train structure with an east-west distribution occurs over the middle and high latitudes of Eurasia when the North Atlantic SST is high, which is typical of positive Eurasian teleconnection pattern (EU)[22], causing an anomalously low pressure over the GD, which leads to anomalously strong westerly winds (Fig. 4c1). When the North Pacific SST is high, the G200 presents a distinct anomaly with a "positive-negative" pattern over East Asia and the Arctic, which is a typical Arctic Oscillation (AO) positive phase[23]. In addition, an abnormal "positive-negative" pattern also appears between the Pacific Ocean and the Arctic,

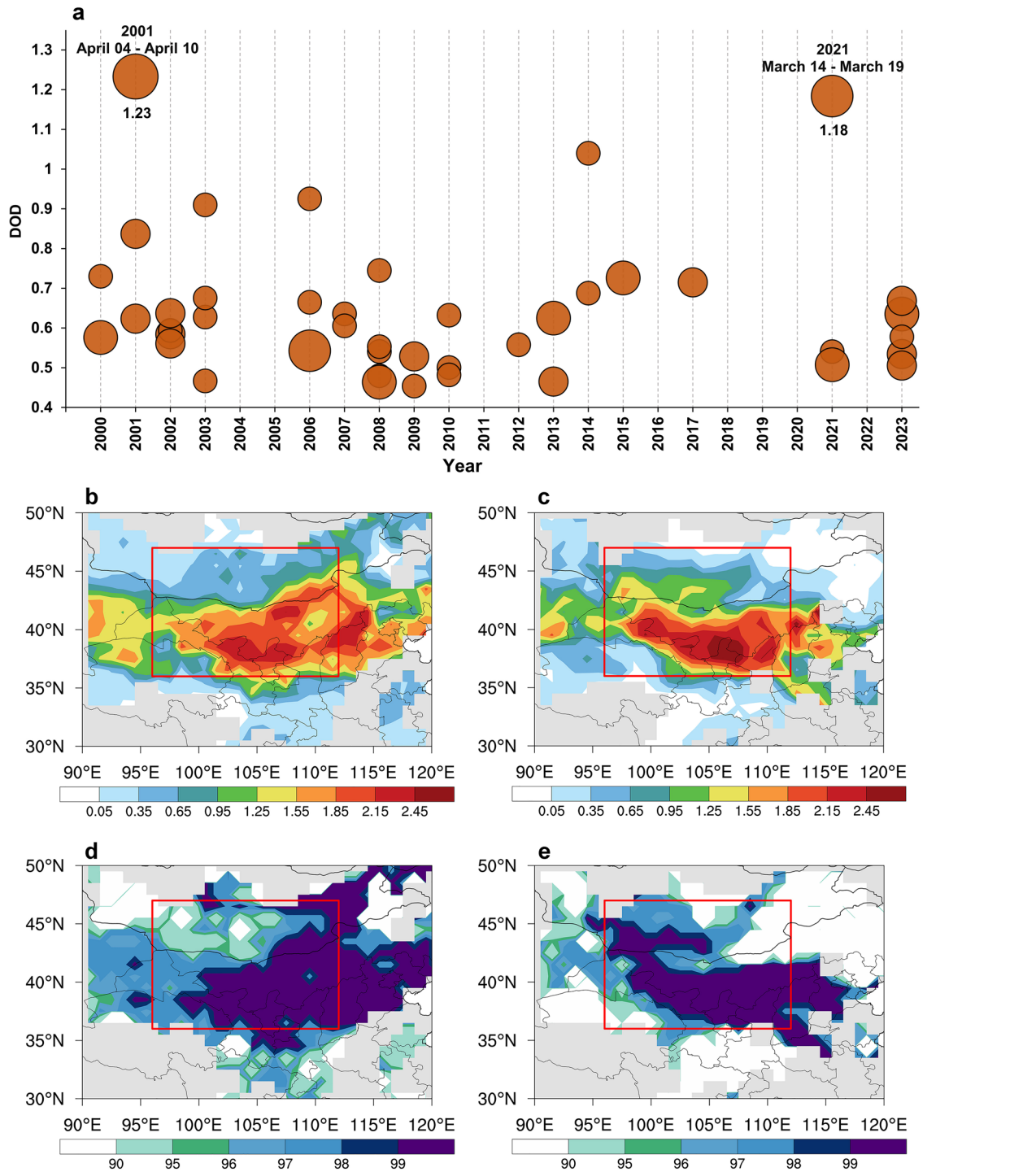

Fig. 1 | Statistics and distributions of EDEs over the GD. a Magnitude and duration of EDEs over the GD (the red rectangle in **b**) in spring from 2000 to 2023. The size of the dots indicates the duration of the events while height denotes the averaged magnitude. The dates and averaged DODs of EDE 2001 and EDE 2021 are shown. Spatial distributions of the averaged DOD during (**b**) EDE 2001 and (**c**) EDE 2021. Percentile of averaged DOD for (**d**) EDE 2001 and (**e**) EDE 2021 during the spring of 2000–2023. The GD is represented by the red rectangle.

which is a typical positive West Pacific teleconnection pattern (WP)[22]. When AO is in the positive phase, the low-pressure over the Arctic is stronger than normal, limiting the southward expansion of cold air, which creates favorable conditions for the abnormal high ST formation over the mid-latitude regions (Fig. 4c2). Moreover, the WP positive phase further promotes abnormal low-pressure over the Arctic region, the wave activity flux indicates that the Rossby waves propagate from the Pacific high-pressure region to the Arctic low-pressure region which further affects the abnormal high pressure over East Asia, leading to the abnormal high ST over the GD (Fig. 4c2). Furthermore, circulations corresponding to SST anomalies are consistent with those corresponding to UV10 and ST (Fig. 4a1 and c1; Fig. 4a2 and c2).

Shift in the dominant factor for EDEs

The above analysis suggests that positive EU associated with high North Atlantic SST strengthens UV10 over the GD, and positive AO and WP due to high North Pacific SST enhances ST over the GD. Accordingly, the indexes representing EU, AO, and WP were calculated[22,23]. Figure 4d shows

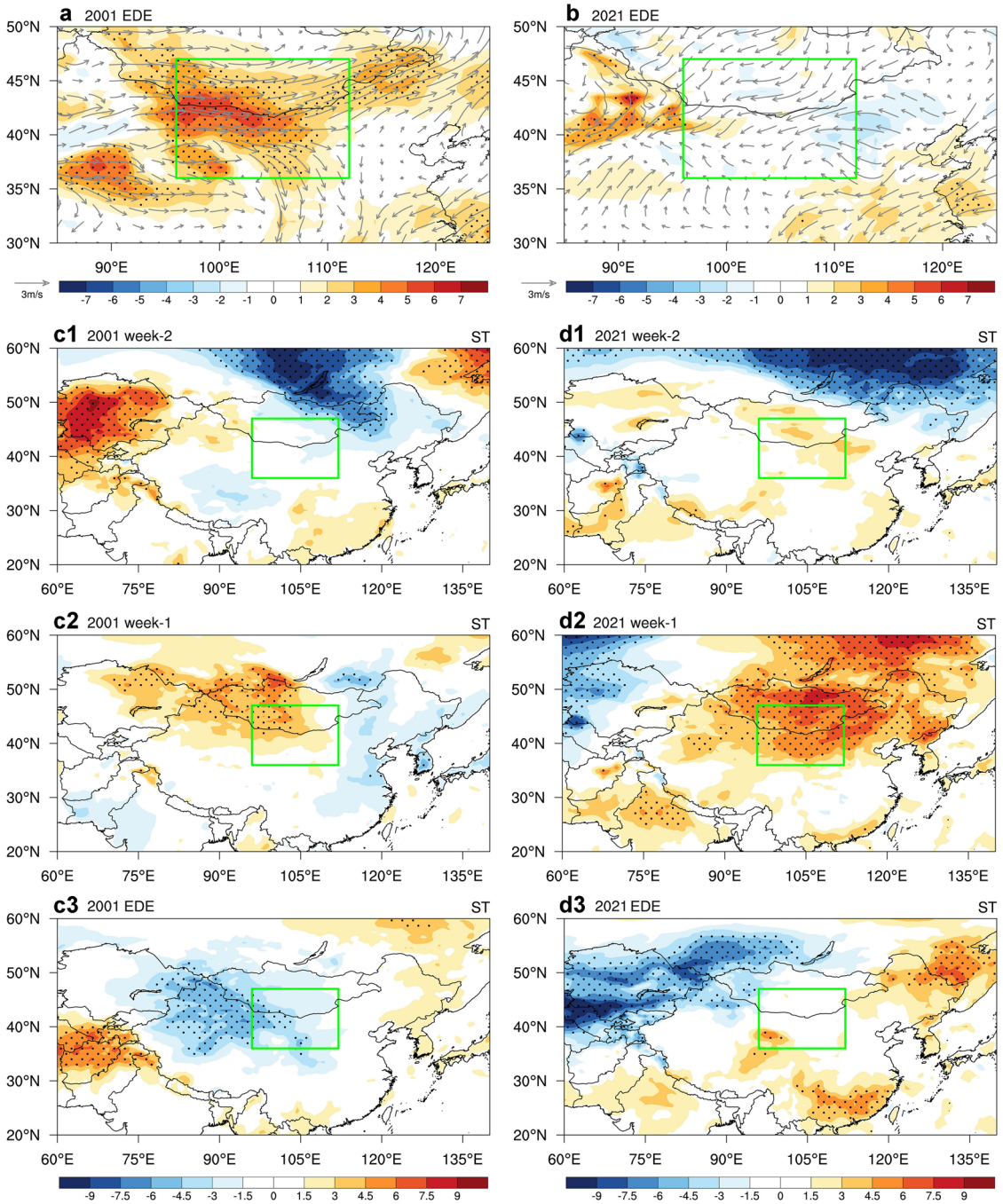

Fig. 2 | Anomalies of UV10 and ST related to EDEs. a Anomalies of 10-m wind vectors (vectors; m s^{-1}) and 10-m wind speeds (shading; m s^{-1}) in EDE 2001 with reference to the 2000–2023 mean value during the same period as EDE 2001 (4–10 April). **b** as in (**a**), but for anomalies in EDE 2021 with reference to the 2000–2023 mean value during the same period as EDE 2021 (14–19 March). (**c1**–**c3**) and (**d1**–**d3**) as in Supplementary Fig. 1(a1–a3) and Supplementary Fig. 1(b1–b3), respectively, but for anomalies of ST (K). "Week-2" and "week-1" denote 2 weeks and 1 week before EDEs, respectively. The dots indicate that the anomalies are significant above the 95% confidence level by the Student's *t*-test. The GD is represented by the green rectangle.

the time series of averaged EUI during 4–10 April (the same period as EDE 2001) from 2000–2023, as well as the time series of averaged AOI and WPI during 7–13 March (the same period as 2021 week-1) from 2000–2023. Corresponding to the years of EDE occurrence, the EUI reached its highest value in 2001 which corresponds to the extreme UV10 that causes EDE 2001, the AOI reached its second highest value as well as the WPI reached its highest value in 2021 which corresponds to the extreme ST and related extreme drought causing EDE 2021. In addition, as depicted in Fig. 4d, the EUI is decreasing, while the AOI and WPI are increasing, suggesting the dominant factor for EDEs over the GD may shift from extreme winds to extreme droughts.

Analysis of meteorological and land conditions during and prior to (1 week) all EDEs confirms the above possibilities. As shown in Fig. 1a, there were a total of 16 years of EDEs during 2000–2023. By dividing these 16 years into groups every four years in chronological order, the meteorological and land conditions of each group were analyzed (Fig. 5). The mean and quartiles of G500 gradually increase from the first to the fourth 4-years prior to (Fig. 5a) and during (Fig. 5b) EDEs, with a corresponding increase in ST during pre-EDEs (Fig. 5c), and a gradual decrease in UV10 during EDEs (Fig. 5d) from the first to the fourth 4-years. The increase in ST and pressure further leads to an increase in soil temperature (Fig. 5e) and decreases in soil water and AI prior to EDEs (Fig. 5f, g) as well as a decrease in NDVI during

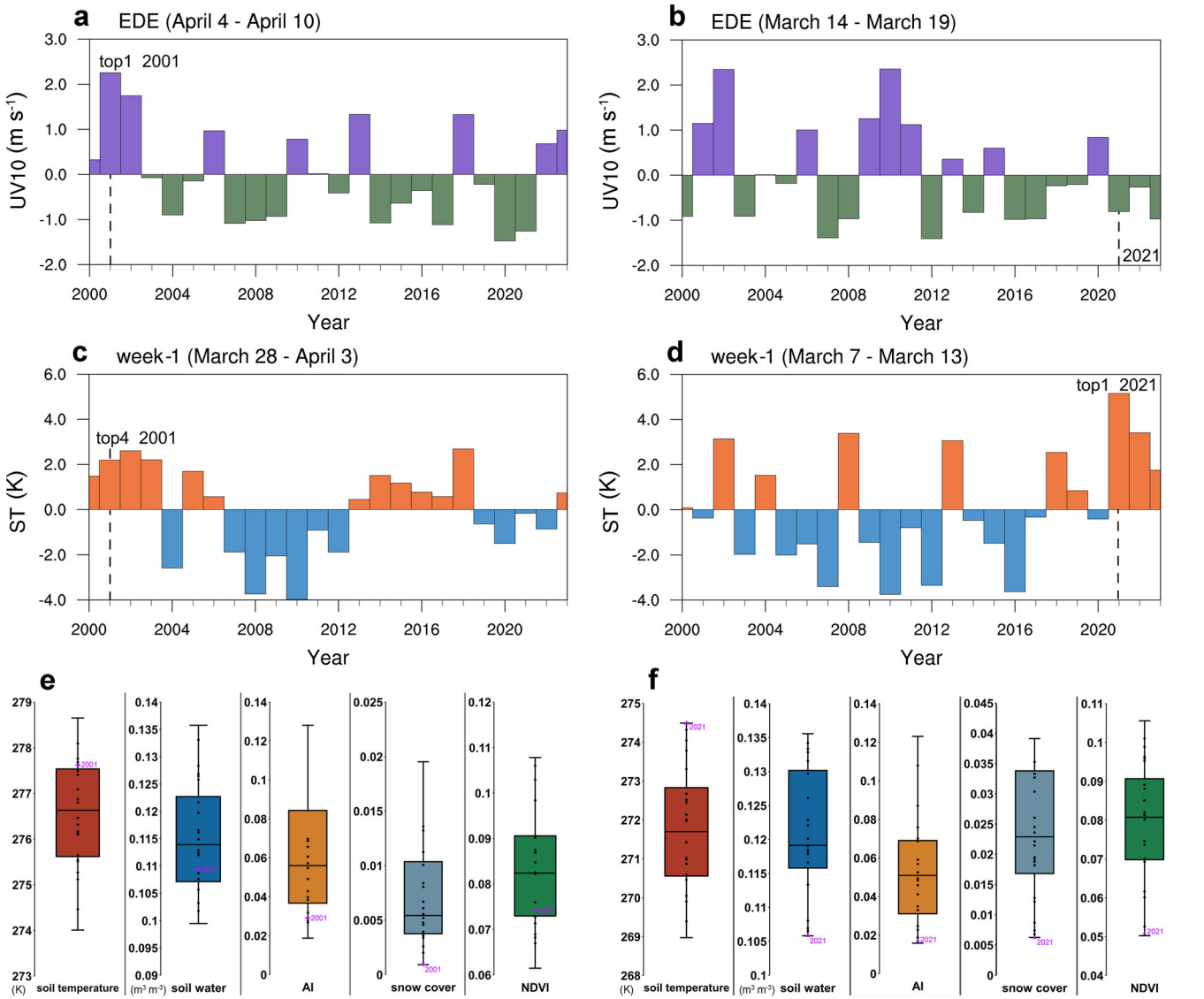

Fig. 3 | Time series of UV10 and ST as well as box plots of surface features associated with EDEs. a Time series of anomalies of UV10 (m s^{-1}) over the GD during 4–10 April (the same period as EDE 2001) from 2000 to 2023. **b** as in (**a**), but for anomalies during 14–19 March (the same period as EDE 2021). **c** Time series of anomalies of ST (K) over the GD during 28 March-3 April (the same period as 2001 week-1) from 2000 to 2023. **d** as in (**c**), but for anomalies during 7–13 March (the same period as 2021 week-1). **e** Box plots of averaged soil temperatures (K), soil water (m^3 m^{-3}), AI, and snow cover during 28 March-3 April (the same period as 2001 week-1) and averaged NDVI during 4–10 April (the same period as EDE 2001) from 2000 to 2023. **f** as in (**e**), but for the periods same as 2021 week-1 and EDE 2021. The ranks of these factors of 2001 and 2021 are marked in purple. Boxes show medians and 25–75% interquartile ranges and whiskers show minimum-maximum ranges.

EDEs (Fig. 5h) from the first to the fourth 4-years. And as time increases, more meteorological and land conditions can reach long-term extreme ranges (light purple shadings in Fig. 5). As shown in Fig. 5a, e–h, more than half of the meteorological and land conditions related to the EDEs in the fourth 4-years lie within the extreme ranges, which is much more than the EDEs in other years. Moreover, the proportions of G500 and UV10 reaching extreme ranges during the EDEs in the fourth 4-years are the lowest (Fig. 5b, d). Thus, droughts in the GD gradually intensified during the pre-EDE period while wind speeds gradually weakened during the EDE period from 2000 to 2023. Combining analysis of the two strongest EDEs, trends in different indices as well as meteorological and land conditions associated with all EDEs, it is detected that the dominant factor of EDEs over the GD is gradually shifting from extreme winds to extreme droughts.

Discussion

Based on satellite observations, EDEs over the GD were identified, and two EDEs with the longest duration and highest intensity were studied in detail. We found that although the duration and intensity of these two EDEs were very similar, the driving factors behind them were different. EDE 2001 was mainly driven by the strongest westerly winds during 2000–2023, which are related to the EU positive phase caused by abnormally warm North Atlantic SST. However, EDE 2021 was mainly caused by the most severe droughts associated with the highest ST in one week before the extreme event during 2000–2023, which is related to the AO positive phase and the WP positive phase due to abnormally warm North Pacific SST.

Previous research on EDEs intensively focused on case studies, with conclusions implying that strong winds and droughts are key to EDEs. Our long-term statistical and comparative analysis of EDEs reveals that the dominant driving factors behind similar EDEs are distinct, and the dominant factor of EDEs is changing. Based on analysis of all EDEs, the generation of EDEs over the GD is increasingly controlled by extremely high pressure and ST, and associated extreme drought is becoming the dominant factor for EDEs. The result highlights the importance of extreme droughts in the production of EDEs, and that extreme droughts should be given more

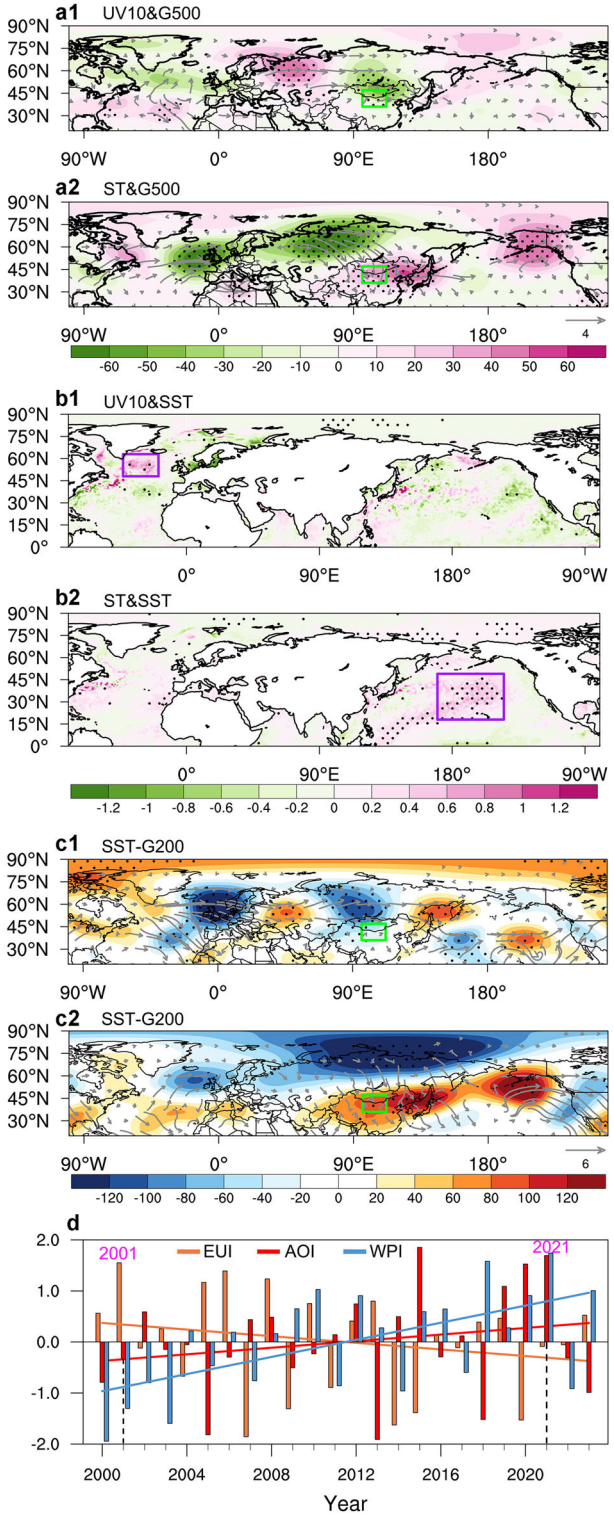

Fig. 4 | Anomalies of G200, Rossby wave, SST, and indexes related to EDEs. Regression patterns of G500 (shading; m) and T-N wave activity flux (vectors; $m^2 s^{-2}$) onto (**a**1) time series of UV10 anomalies during 4–10 April (same period as EDE 2001) from 2000–2023 and (**a**2) time series of ST anomalies during 7–13 March (same period as 2021 week-1) from 2000–2023. **b**1 and (**b**2) as in (**a**1) and (**a**2), but for regression patterns of SST (°C). The purple rectangle represents the area for calculating the average SST. The green rectangle represents the GD. **c**1 and (**c**2) represent anomalies in G200 and T-N wave activity flux during high North Atlantic SST years and high North Pacific SST years, respectively. The dots indicate the regressions and differences are significant above the 95% confidence level by the Student's *t*-test. **d** represents the time series of standardized EUI averaged during 4–10 April (same period as EDE 2001), AOI and WPI averaged during 7–13 March (same period as 2021 week-1) from 2000 to 2023. Solid lines represent linear fits.

attention in future predictions of EDEs. Moreover, increased droughts in arid and semi-arid regions as a result of global warming will severely exacerbate the occurrence of EDEs, and therefore necessary and effective climate action is key to curbing this situation.

Methods

Observations

The Moderate Resolution Imaging Spectroradiometer (MODIS) onboard the Terra satellite provides aerosol observations since 2000, including aerosol optical depths (AOD), Ångström exponent (AE), and single scattering albedo (SSA). Based on the size distribution and absorption characteristics of dust particles, Pu and Ginoux[24] derived a formula for calculating DOD over land:

$$\mathrm{DOD} = \mathrm{AOD}_{550\mathrm{nm}} \times (0.98 - 0.508 \times \mathrm{AE} + 0.051 \times \mathrm{AE}^2) \quad (1)$$

In addition, the formula requires SSA at 470 nm to be less than 0.99 for the retrieval of DOD. This method has been widely applied in dust-related studies[14,25,26]. The aerosol observations in this study come from the MODIS Collection 6.1 daily average product (MOD08), which was derived using the Deep Blue algorithm[27].

NOAA Climate Data Records (CDRs) provide long-term land, oceans, atmosphere, and ice datasets. The Optimum Interpolation Sea Surface Temperature (OISST)[28] from CDRs is a comprehensive climate data which incorporates observations from various platforms into a regular global grid. In this study, we used the daily SST data provided by OISST, with a resolution of 0.25°. Moreover, the daily NDVI from NOAA CDRs with a resolution of 0.05° is used in this study[29].

Reanalysis data

The hourly meteorological and land conditions related to dust events, including UV10, ST, G500, G200, winds at 850 hPa (UV850), soil temperature, soil water, potential evaporation, and precipitation are derived from ERA5 reanalysis datasets[30–33], with a resolution of 0.5°. The ratio of precipitation to potential evaporation is used as AI. The calculation of Rossby wave activity flux is based on Takaya and Nakamura[34]. The hourly snow cover fraction is derived from MERRA-2 reanalysis datasets[35], with a resolution of 0.5° × 0.625° (latitude × longitude). Moreover, according to previous studies, these reanalysis data have excellent applicability to extreme weather events[36,37].

Identification of extreme dust events

According to Pu and Jin[6], we defined an EDE over the GD (the area surrounded by the red rectangle in Fig. 1b; 36–47°N, 96–112°E) as when regional averaged daily DOD is greater than the 90th percentile of daily DOD during the spring (March to May) of 2000–2023. Within the scope of an EDE, the number of continuous days (at least 2 days) is the standard for the duration of an EDE. The strength of an EDE is calculated as the DOD averaged over all days during the event. There are a total of 2208 days in the spring of 2000 to 2023, of which 2177 days were available for detecting DOD data, and the calculated DOD threshold is 0.446.

Statistical significance test

In this study, correlation and regression are used to measure the relationship between two variables, and the significance test is based on the two-sided Student's *t*-test.

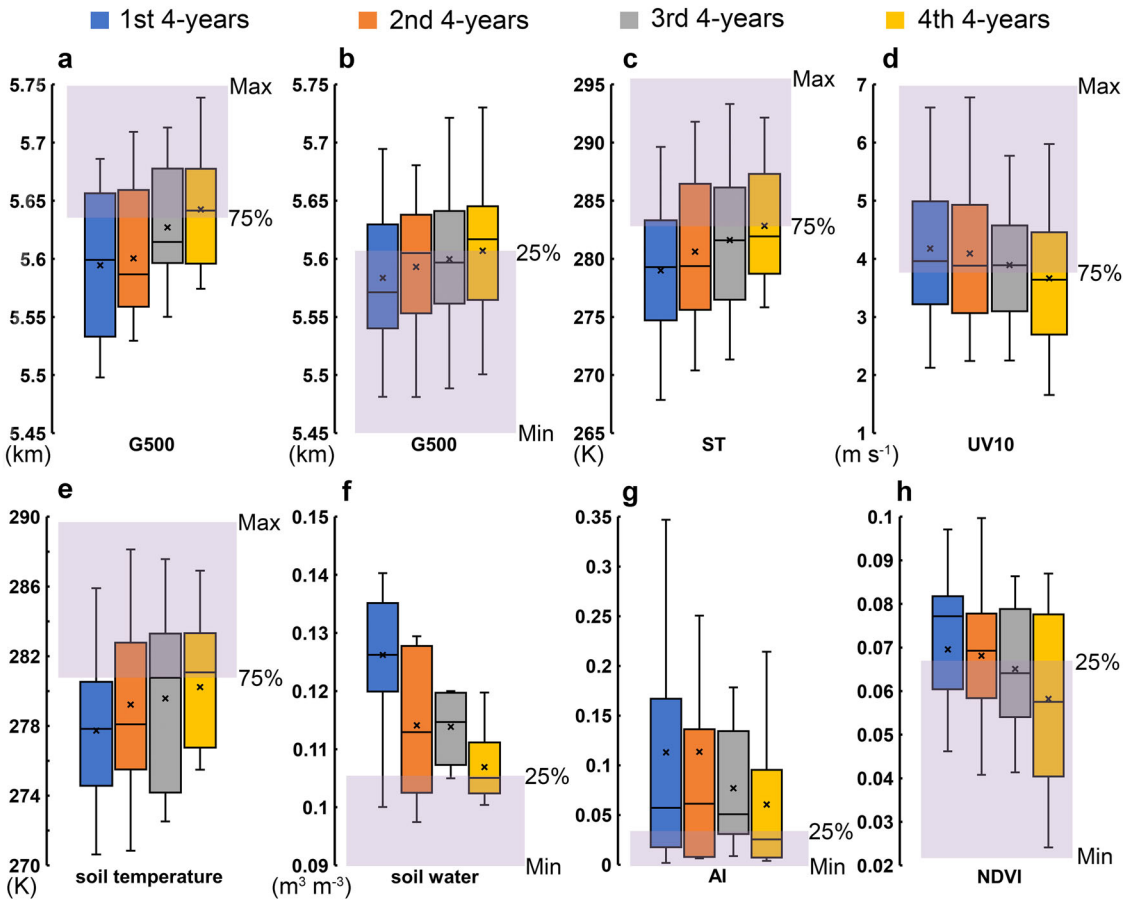

Fig. 5 | Meteorological and land conditions over the GD associated with EDEs at different periods. a Box plot of averaged G500 (km) during each pre-EDE at different time periods. **b** Box plot of averaged G500 (km) during each EDE at different time periods. **c** Box plot of averaged ST (K) during each pre-EDE at different periods. **d** Box plot of averaged UV10 (m s^{-1}) during each EDE at different periods. **e**–**g** Box plots of averaged Soil temperature (K), soil water (m^3 m^{-3}), and AI during each pre-EDE at different periods. **h** Box plot of averaged NDVI during each EDE at different periods (boxes show medians and 25–75% interquartile ranges, asterisks show mean values and whiskers show minimum-maximum ranges). Pre-EDE is defined as one week before the first day of EDE. According to Fig. 1a, the 1st 4-years include 2000, 2001, 2002, and 2003, the 2nd 4-years include 2006, 2007, 2008, and 2009, the 3rd 4-years include 2010, 2012, 2013, and 2014, the 4th 4-years include 2015, 2017, 2021, and 2023. The light purple shading represents the 25% quantile to minimum or 75% quantile to maximum of daily mean values of each variable during the same period as EDEs or pre-EDEs from 2000 to 2023.

Data availability

ERA5 reanalysis data were obtained from https://cds.climate.copernicus.eu/cdsapp#!/dataset/reanalysis-era5-pressure-levels?tab=form, MERRA-2 reanalysis data were obtained from https://goldsmr4.gesdisc.eosdis.nasa.gov/data/MERRA2/M2T1NXLND.5.12.4/. MODIS observations were downloaded from https://ladsweb.modaps.eosdis.nasa.gov/archive/allData/61/MOD08_D3. OISST and NDVI data were obtained from https://www.ncei.noaa.gov/data/sea-surface-temperature-optimum-interpolation/v2.1/access/avhrr/ and https://www.ncei.noaa.gov/data/land-normalized-difference-vegetation-index/access/, respectively.

Code availability

Codes for this study are available upon reasonable requests from the corresponding author.

Received: 2 April 2024; Accepted: 9 June 2024;
Published online: 19 June 2024

References

1. Wang, J. et al. Anthropogenically-driven increases in the risks of summertime compound hot extremes. *Nat. Commun.* **11**, 1–11 (2020).
2. Cohen, J., Agel, L., Barlow, M., Garfinkel, C. & White, I. Linking Arctic variability and change with extreme winter weather in the United States. *Science* **373**, 1116–1121 (2021).
3. Zhou, S., Yu, B. F. & Zhang, Y. Global concurrent climate extremes exacerbated by anthropogenic climate change. *Sci. Adv.* **9**, eabo1638 (2023).
4. IPCC. *Climate Change 2022: Impacts, Adaptation, and Vulnerability. Contribution of Working Group II to the Sixth Assessment Report of the Intergovernmental Panel on Climate Change. Climate Change 2022 – Impacts, Adaptation and Vulnerability* (Cambridge Univ. Press, 2022).
5. World Meterological Organization (WMO). *Atlas of mortality and economic losses from weather, climate and water extremes (1970-2019). WMO-No. 1267*. https://library.wmo.int/idurl/4/57564 (2021).
6. Pu, B. & Jin, Q. A record-breaking trans-Atlantic African dust plume associated with atmospheric circulation extremes in June 2020. *B. Am. Meteorol. Soc.* **102**, E1340–E1356 (2021).
7. Singh, C., Singh, S. K., Chauhan, P. & Budakoti, S. Simulation of an extreme dust episode using WRF-CHEM based on optimal ensemble approach. *Atmos. Res.* **249**, 105296 (2021).
8. Zittis, G. et al. Climate change and weather extremes in the Eastern Mediterranean and Middle East. *Rev. Geophys.* **60**, e2021RG000762 (2022).
9. Li, J. et al. Predominant type of dust storms that influences air quality over northern China and future projections. *Earth's Future* **10**, e2022EF002649 (2022).

10. Yin, Z., Wan, Y., Zhang, Y. & Wang, H. Why super sandstorm 2021 in north China? *Natl. Sci. Rev.* **9**, nwab165 (2022).
11. Chen, S. et al. Mongolia contributed more than 42% of the dust concentrations in Northern China in March and April 2023. *Adv. Atmos. Sci.* **40**, 1–9 (2023).
12. Yin, Z. et al. Mechanisms of dust source accumulation and synoptic disturbance triggering 331 the 2023 spring sandstorm in Northern China (in Chinese). *Trans. Atmos. Sci.* **46**, 321–331 (2023).
13. Liu, S. et al. Wind-blown dust and its impacts on particulate matter pollution in northern China: current and future scenario. *Environ. Res. Lett.* **16**, 114041 (2021).
14. Gui, K. et al. Record-breaking dust loading during two mega dust storm events over northern China in March 2021: Aerosol optical and radiative properties and meteorological drivers. *Atmos. Chem. Phys.* **22**, 7905–7932 (2022).
15. Zhao, X., Huang, K., Fu, J. S. & Abdullaev, S. F. Long-range transport of Asian dust to the Arctic: identification of transport pathways, evolution of aerosol optical properties, and impact assessment on surface albedo changes. *Atmos. Chem. Phys.* **22**, 10389–10407 (2022).
16. Duan, B. et al. Cause analysis on severe dust storm in Northern China on 15 March 2021 (in Chinese). *Arid Meteor.* **39**, 541–553 (2021).
17. Yang, X. et al. Characteristics and causes of persistent sand-dust weather in mid-March 2021 over Northern China (in Chinese). *Desert Res.* **41**, 245–255 (2021).
18. Zhang, R., Han, Z., Wang, M. & Zhang, X. Dust storm weather in China: new characteristics and origins (in Chinese). *Quat. Sci.* **22**, 374–380 (2002).
19. Zhang, Z., Wang, K., Chen, D., Li, J. & Dickinson, R. Increase in surface friction dominates the observed surface wind speed decline during 1973–2014 in the Northern Hemisphere Lands. *J. Clim.* **32**, 7421–7435 (2019).
20. Cook, B. I. et al. Twenty-firstcentury drought projections in the CMIP6 forcing scenarios. *Earth's Future* **8**, e2019EF001461 (2020).
21. Yuan, X. et al. A global transition to flash droughts under climate change. *Science* **380**, 187–191 (2023).
22. Wallace, J. M. & Gutzler, D. S. Teleconnections in the geopotential height field during the Northern Hemisphere winter. *Mon. Weather Rev.* **109**, 784–812 (1981).
23. Thompson, D. W. J. & Wallace, J. M. The Arctic Oscillation signature in the wintertime geopotential height and temperature fields. *Geophys. Res. Lett.* **25**, 1297–1300 (1998).
24. Pu, B. & Ginoux, P. How reliable are CMIP5 models in simulating dust optical depth? *Atmos. Chem. Phys.* **18**, 12491–12510 (2018).
25. Song, Q., Zhang, Z., Yu, H., Ginoux, P. & Shen, J. Global dust optical depth climatology derived from CALIOP and MODIS aerosol retrievals on decadal timescales: regional and interannual variability. *Atmos. Chem. Phys.* **21**, 13369–13395 (2021).
26. Han, Y. et al. CALIOP-based quantification of central asian dust transport. *Remote Sens.* **14**, 1416 (2022).
27. Levy, R. C. et al. The Collection 6 MODIS aerosol products over land and ocean. *Atmos. Meas. Tech.* **6**, 2989–3034 (2013).
28. Huang, B. Y. et al. Improvements of the daily optimum interpolation sea surface temperature (DOISST) version 2.1. *J. Clim.* **34**, 2923–2939 (2021).
29. Vermote, E. NOAA CDR Program: NOAA Climate Data Record (CDR) of AVHRR Normalized Difference Vegetation Index (NDVI), Version 5. *NOAA National Centers for Environmental Information*. https://doi.org/10.7289/V5ZG6QH9 (2019).
30. Hersbach, H. et al. The ERA5 global reanalysis. *Q. J. Roy. Meteor. Soc.* **146**, 1999–2049 (2020).
31. Xia, Y. et al. Stratospheric ozone loss enhances summer precipitation over the southern slope of the Tibetan Plateau. *Geophys. Res. Lett.* **50**, e2023GL103742 (2023).
32. Tan, Z. et al. Association between Tibetan heat sources and heat waves in China. *J. Climate.* **36**, 7905–7924 (2023).
33. Sun, Y. et al. Microphysical characteristics of precipitation over Eastern China and its coastal regions. *Journal of Geophysical Research: Atmospheres.* **129**, e2023JD039817 (2024).
34. Takaya, K. & Nakamura, H. A formulation of a phase-independent wave-activity flux for stationary and migratory quasigeostrophic eddies on a zonally varying basic flow. *J. Atmos. Sci.* **58**, 608–627 (2001).
35. Randles, C. A. et al. The MERRA-2 aerosol reanalysis, 1980-onward, Part I: System description and data assimilation evaluation. *J. Clim.* **30**, 6823–6850 (2017).
36. Xiao, H., Xu, P. & Wang, L. The unprecedented 2023 North China heatwaves and their S2S predictability. *Geophys. Res. Lett.* **51**, e2023GL107642 (2024).
37. Xia, Y. et al. Concurrent hot extremes and high ultraviolet radiation in summer over the Yangtze Plain and their possible impact on surface ozone. *Environ. Res. Lett.* **17**, 064001 (2022).

Acknowledgements

This research was supported by the Shandong Provincial Natural Science Foundation (ZR2023QD169), the Fundamental Research Funds for the Central Universities (202313022), the Second Tibetan Plateau Scientific Expedition and Research Program (2019QZKK0602), and the National Natural Science Foundation of China (41991231).

Author contributions

Q.Z. designed the study and performed the research; Y.L. provided a computing platform and improvement suggestions for the research. All authors contributed to interpreting results, discussion, and improvement of this paper.

Competing interests

The authors declare no competing interests.

Additional information

Supplementary information The online version contains

supplementary material available at https://doi.org/10.1038/s41612-024-00689-z.

Correspondence and requests for materials should be addressed to Yuzhi Liu.